Center for Optical Technologies
All-Optical Functionalities
FUNDAMENTALS • MATERIALS • EFFECTS
THRUST

LEHIGH UNIVERSITY
Northampton Community College
PENNSTATE 1855
Lehigh Carbon COMMUNITY COLLEGE
Ben Franklin Technology PArtners

Development and Photonic Application Potentials of Zinc Oxide Single Crystal Microtubes

Jiping Cheng, Y. Fu, H.Y. Wang, A. Skrabut, and Ruyan Guo
Materials Research Institute and Dept. Electrical Engineering, Penn State University
University Park, PA 16802

ZnO

A promising material for next generation of opto-electronic applications.

APPLICATIONS of ZnO MATERIALS

Traditional Applications:
(from powder and polycrystalline Ceramic)

- Phosphors
- Catalysts
- Gas Sensors
- Varistors
- Piezoelectric Transducers

Advanced Applications:
(from single crystals or nanorods/wires)

- High Temperature Transistors
- UV Light Detectors
- Electrooptic Devices
- Blue and UV Light Emitting Diodes (LEDs)
- Blue and UV Lasers (LDs)

Structural and Physical Properties of ZnO

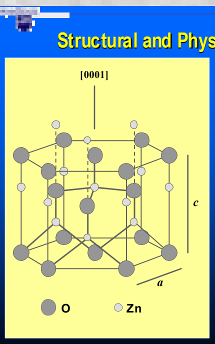

Wurtzite structure

Hexagonal crystal system
crystal class *6mm*,
a=3.24982, c=5.20661

Melting point = 1975°C
Density = 5.606 g/cm^3
Hardness = 4-5 Moh scale
Thermal conductivity
0.006 Cal/cm°K
Thermal expansion = 2.90x10^{-6}/K

E_{gap} = 3.4 eV (λ= 365 nm)

Free exciton binding energy
60 meV

ZnO Microtubes

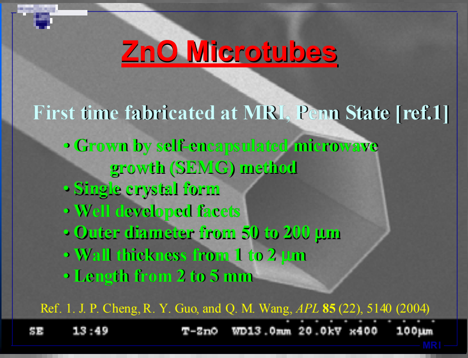

First time fabricated at MRI, Penn State [ref.1]

- Grown by self-encapsulated microwave growth (SEMG) method
- Single crystal form
- Well developed facets
- Outer diameter from 50 to 200 µm
- Wall thickness from 1 to 2 µm
- Length from 2 to 5 mm

Ref. 1. J. P. Cheng, R. Y. Guo, and Q. M. Wang, *APL* **85** (22), 5140 (2004)

Morphology of the ZnO single crystal microtubes made by SEMG

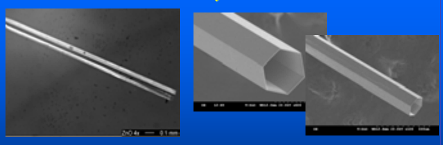

(a) Optical microscope image shows colorless and highly transparent ZnO microtubes.

(b) SEM pictures reveal that the ZnO crystals are grown with a hexagonal hollow tubular texture of well faceted ends and side surfaces.

Laue back reflection patterns from the wall side {1100} of the ZnO single crystal tube

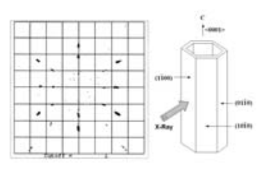

The XRD pattern revealed that the ZnO single crystal tubes grow along the <0001> direction with six {1100} planes joined at the {1000} mirror plane forming a perfect hexagon

Physical Properties of the ZnO single crystal microtubes (a) Light emission properties

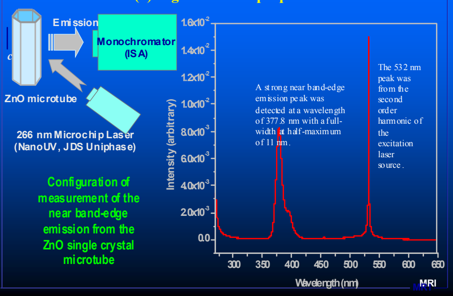

A strong near band-edge emission peak was detected at a wavelength of 377.8 nm with a full-width at half-maximum of 11 nm.

The 532 nm peak was from the second order harmonic of the excitation laser source.

Configuration of measurement of the near band-edge emission from the ZnO single crystal microtube

Physical Properties of the ZnO single crystal microtubes (b) UV photoresponse properties

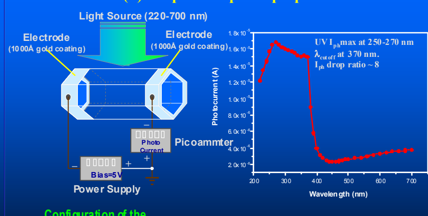

UV I_{ph}max at 250-270 nm
$\lambda_{cut off}$ at 370 nm.
I_{ph} drop ratio ~ 8

Configuration of the photoresponse measurement on the ZnO single crystal microtube

The photoresponse spectra of the ZnO single crystal microtubes

Physical Properties of the ZnO single crystal microtubes (c) Field emission properties

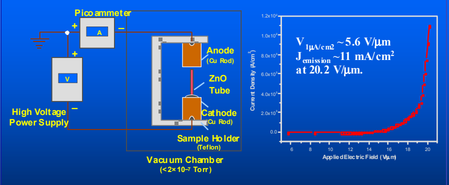

$V_{1\mu A/cm2}$ ~5.6 V/µm
$J_{emission}$ ~11 mA/cm^2
at 20.2 V/µm.

Configuration of the field emission measurement on the ZnO single crystal microtube

Field emission properties of the ZnO single crystal microtubes

Piezoelectric d_{33} Determination by Optical Laser Dilatometry

Single Beam Interferometer

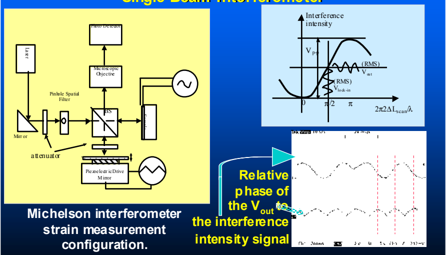

Michelson interferometer strain measurement configuration.

Relative phase of the V_{out} to the interference intensity signal

Sample configuration – one end clamped c-axis hollow rod in longitudinal E-field.

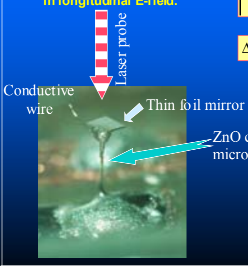

$$d_{33} = \frac{\lambda}{2\sqrt{2}}\frac{V_{OUT}}{V_{lock-in}\cdot V_{P-P}}$$

$$\Delta L = d_{33}E\cdot L_0 = d_{33}\cdot V_{lock-in}$$

Expected Resonances:
Medium Diameter – 9 MHz
Wall Thickness – 2.2. GHz
Length – 2.1 MHz
Displacement < 1 nm in weak electric field.

Longitudinal Strain and Effective d_{33} as Function of Frequency

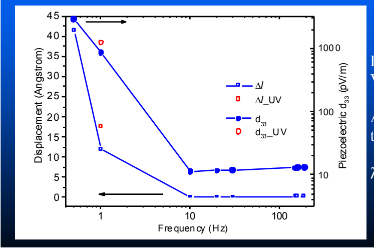

E~1.5 V/mm

At room temp.

λ=633 nm

Gaint Static d_{33}

Enormously large effective d_{33} values were obtained under low frequency (<10 Hz) and weak electric field (2 V/mm peak-to-peak) conditions.

Effective d_{33} showed strong frequency dependence tapering off rapidly with increasing frequency to 11-13 pC/N (similar to bulk crystal, 12 pC/N by resonance technique [ref.2]).

UV illumination on sample increases the longitudinal strain and the apparent d_{33}, indicating enhancement effect of non-equilibrium carrier on d_{33} through photostriction at low frequencies.

Ref. 2. A.R. Butson, *Phys. Rev. Lett.* **4**(10) 505 (1960)

Simulation of Static Piezoelectric Strain in Hexagonal ZnO Microtubes

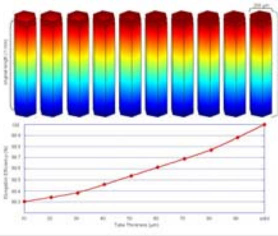

FEMLAB simulation shows that decreasing tubular wall thickness results in decreased longitudinal strain – due to negative d_{31}.

Effect of Complex Radial Modes in Hollow Hexagonal Structure on Effective d_{33}

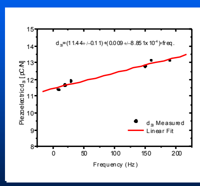

Increasing trend of effective d_{33} with frequency was obtained for 10<freq.<200 Hz measured. Simulations on longitudinal displacement indicates that the complex radial (wall thickness and tubular OD and ID diameters) modes can make positive or negative contribution to the effective d_{33}. Further studies are being carried out currently.

Conclusions

Self-encapsulated microwave growth method has been reported recently by Cheng et al. as an unique technique for growth of high quality ZnO single crystal microtubes.

The effective longitudinal piezoelectric properties of ZnO microtubes were studied using an optical laser dilatometry method based on single beam interferometer in Michelson configuration.

Enormously large effective d_{33} values (>1000 pC/N) in low frequency were obtained, which tapers off quickly with increasing frequency.

ZnO microtubes have comparable piezoelectric d_{33} compared to bulk crystals; however showing increasing trend with frequency within the measurement range.

Influence of complex radial modes on effective d_{33} is currently being studied using finite element analysis.

Acknowledgement

William White on photoresponse measurements
Jeremy Acord on photoluminescence measurement
Amar Bhalla on concepts and discussion

Partial support:
PA Center for Optical Technology
NSF Grant No. DMI-0322286
NSF Grant No. EEC-2044030

MRI